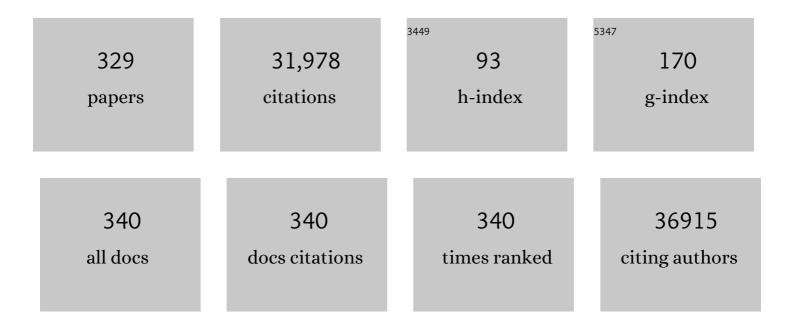
Joel W Ager

List of Publications by Year in descending order

Source: https://exaly.com/author-pdf/2076490/publications.pdf Version: 2024-02-01



LOFI W ACER

#	Article	IF	CITATIONS
1	Surface Reconstruction of Perovskites for Water Oxidation: The Role of Initial Oxides' Bulk Chemistry. Small Science, 2022, 2, 2100048.	5.8	21
2	Minor Product Polymerization Causes Failure of High-Current CO ₂ -to-Ethylene Electrolyzers. ACS Energy Letters, 2022, 7, 599-601.	8.8	10
3	Reversible Photochromism in ⟠110⟩ Oriented Layered Halide Perovskite. ACS Nano, 2022, 16, 2942-2952.	7.3	23
4	Alkali Additives Enable Efficient Large Area (>55 cm ²) Slotâ€Die Coated Perovskite Solar Modules. Advanced Functional Materials, 2022, 32, .	7.8	39
5	Giant Isotope Effect of Thermal Conductivity in Silicon Nanowires. Physical Review Letters, 2022, 128, 085901.	2.9	16
6	Energy Spotlight. ACS Energy Letters, 2022, 7, 1574-1576.	8.8	0
7	The 2022 solar fuels roadmap. Journal Physics D: Applied Physics, 2022, 55, 323003.	1.3	58
8	Theory of liquid-mediated strain release in two-dimensional materials. Physical Review Materials, 2022, 6, .	0.9	1
9	Elucidating Reaction Pathways of the CO ₂ Electroreduction via Tailorable Tortuosities and Oxidation States of Cu Nanostructures. Advanced Functional Materials, 2022, 32, .	7.8	9
10	Copper sulfide as the cation exchange template for synthesis of bimetallic catalysts for CO ₂ electroreduction. RSC Advances, 2021, 11, 23948-23959.	1.7	6
11	Photophysics of Localized Deep Defect States in Hybrid Organic–Inorganic Perovskites. Journal of Physical Chemistry C, 2021, 125, 6975-6982.	1.5	2
12	A discussion on the possible involvement of singlet oxygen in oxygen electrocatalysis. JPhys Energy, 2021, 3, 031004.	2.3	31
13	Spin pinning effect to reconstructed oxyhydroxide layer on ferromagnetic oxides for enhanced water oxidation. Nature Communications, 2021, 12, 3634.	5.8	186
14	Carbon neutral manufacturing via on-site CO2 recycling. IScience, 2021, 24, 102514.	1.9	29
15	Tandem Electrocatalytic CO ₂ Reduction with Efficient Intermediate Conversion over Pyramid-Textured Cu–Ag Catalysts. ACS Applied Materials & Interfaces, 2021, 13, 40513-40521.	4.0	23
16	Manipulating Intermediates at the Au–TiO ₂ Interface over InP Nanopillar Array for Photoelectrochemical CO ₂ Reduction. ACS Catalysis, 2021, 11, 11416-11428.	5.5	48
17	Economically viable CO ₂ electroreduction embedded within ethylene oxide manufacturing. Energy and Environmental Science, 2021, 14, 1530-1543.	15.6	24
18	Wetting-regulated gas-involving (photo)electrocatalysis: biomimetics in energy conversion. Chemical Society Reviews, 2021, 50, 10674-10699.	18.7	63

#	Article	IF	CITATIONS
19	Active Phase on SrCo _{1–<i>x</i>} Fe _{<i>x</i>} O _{3â^îî} (0 ≤i>x ≤ Perovskite for Water Oxidation: Reconstructed Surface versus Remaining Bulk. Jacs Au, 2021, 1, 108-115.).5) 3.6	47
20	Effects of surface diffusion in electrocatalytic CO2 reduction on Cu revealed by kinetic Monte Carlo simulations. Journal of Chemical Physics, 2021, 155, 164701.	1.2	7
21	Techno-economic assessment of emerging CO2 electrolysis technologies. STAR Protocols, 2021, 2, 100889.	0.5	11
22	Solar-Driven Gas-Phase Moisture to Hydrogen with Zero Bias. ACS Nano, 2021, 15, 19119-19127.	7.3	16
23	Design principles of tandem cascade photoelectrochemical devices. Sustainable Energy and Fuels, 2021, 5, 6361-6371.	2.5	6
24	Investigation and mitigation of degradation mechanisms in Cu2O photoelectrodes for CO2 reduction to ethylene. Nature Energy, 2021, 6, 1124-1132.	19.8	85
25	Lattice site–dependent metal leaching in perovskites toward a honeycomb-like water oxidation catalyst. Science Advances, 2021, 7, eabk1788.	4.7	41
26	The Bright Side and Dark Side of Hybrid Organic–Inorganic Perovskites. Journal of Physical Chemistry C, 2020, 124, 27340-27355.	1.5	3
27	Heterogenized Pyridine-Substituted Cobalt(II) Phthalocyanine Yields Reduction of CO ₂ by Tuning the Electron Affinity of the Co Center. ACS Applied Materials & Interfaces, 2020, 12, 5251-5258.	4.0	41
28	Enhancement of the photoelectrochemical water splitting by perovskite BiFeO3 via interfacial engineering. Solar Energy, 2020, 202, 198-203.	2.9	49
29	Surface Composition Dependent Ligand Effect in Tuning the Activity of Nickel–Copper Bimetallic Electrocatalysts toward Hydrogen Evolution in Alkaline. Journal of the American Chemical Society, 2020, 142, 7765-7775.	6.6	234
30	Research advances towards large-scale solar hydrogen production from water. EnergyChem, 2019, 1, 100014.	10.1	130
31	Machine Learning Optimization of p-Type Transparent Conducting Films. Chemistry of Materials, 2019, 31, 7340-7350.	3.2	30
32	Sequential Cascade Electrocatalytic Conversion of Carbon Dioxide to C–C Coupled Products. ACS Applied Energy Materials, 2019, 2, 4551-4559.	2.5	64
33	Electrical suppression of all nonradiative recombination pathways in monolayer semiconductors. Science, 2019, 364, 468-471.	6.0	243
34	Si photocathode with Ag-supported dendritic Cu catalyst for CO ₂ reduction. Energy and Environmental Science, 2019, 12, 1068-1077.	15.6	93
35	Exceptionally active iridium evolved from a pseudo-cubic perovskite for oxygen evolution in acid. Nature Communications, 2019, 10, 572.	5.8	254
36	Spatially Precise Transfer of Patterned Monolayer WS ₂ and MoS ₂ with Features Larger than 10 ⁴ μm ² Directly from Multilayer Sources. ACS Applied Electronic Materials, 2019, 1, 407-416.	2.0	23

 $\mathsf{JOEL}\,\mathsf{W}\,\mathsf{AGER}$

#	Article	IF	CITATIONS
37	Evidence for product-specific active sites on oxide-derived Cu catalysts for electrochemical CO2 reduction. Nature Catalysis, 2019, 2, 86-93.	16.1	212
38	Synthetic WSe ₂ monolayers with high photoluminescence quantum yield. Science Advances, 2019, 5, eaau4728.	4.7	78
39	Deterministic Assembly of Arrays of Lithographically Defined WS2 and MoS2 Monolayer Features Directly From Multilayer Sources Into Van Der Waals Heterostructures. Journal of Micro and Nano-Manufacturing, 2019, 7, .	0.8	12
40	The Technical and Energetic Challenges of Separating (Photo)Electrochemical Carbon Dioxide Reduction Products. Joule, 2018, 2, 381-420.	11.7	148
41	Investigating the Role of Copper Oxide in Electrochemical CO ₂ Reduction in Real Time. ACS Applied Materials & Materials & Applied & Applied Materials & Applied & App	4.0	207
42	Operando Investigation of Mn ₃ O _{4+î´} Co-catalyst on Fe ₂ O ₃ Photoanode: Manganese-Valency-Determined Enhancement at Varied Potentials. ACS Applied Energy Materials, 2018, 1, 814-821.	2.5	21
43	Large-area and bright pulsed electroluminescence in monolayer semiconductors. Nature Communications, 2018, 9, 1229.	5.8	146
44	Ultrahigh thermal conductivity of isotopically enriched silicon. Journal of Applied Physics, 2018, 123, .	1.1	21
45	Scientific and Technological Assessment of Iron Pyrite for Use in Solar Devices. Energy Technology, 2018, 6, 8-20.	1.8	21
46	Solutionâ€Processed Transparent Selfâ€Powered pâ€CuSâ€ZnS/nâ€ZnO UV Photodiode. Physica Status Solidi - Rapid Research Letters, 2018, 12, 1700381.	1.2	54
47	Stability of Residual Oxides in Oxideâ€Derived Copper Catalysts for Electrochemical CO ₂ Reduction Investigated with ¹⁸ O Labeling. Angewandte Chemie - International Edition, 2018, 57, 551-554.	7.2	300
48	Initial Application of Selectedâ€Ion Flowâ€Tube Mass Spectrometry to Realâ€Time Product Detection in Electrochemical CO ₂ Reduction. Energy Technology, 2018, 6, 110-121.	1.8	13
49	Stability of Residual Oxides in Oxideâ€Derived Copper Catalysts for Electrochemical CO 2 Reduction Investigated with 18 O Labeling. Angewandte Chemie, 2018, 130, 560-563.	1.6	43
50	Metal–Oxygen Hybridization Determined Activity in Spinel-Based Oxygen Evolution Catalysts: A Case Study of ZnFe _{2–<i>x</i>} Cr _{<i>x</i>} O ₄ . Chemistry of Materials, 2018, 30, 6839-6848.	3.2	65
51	Chemical storage of renewable energy. Science, 2018, 360, 707-708.	6.0	150
52	Sequential catalysis controls selectivity in electrochemical CO ₂ reduction on Cu. Energy and Environmental Science, 2018, 11, 2935-2944.	15.6	165
53	Electrochemical CO Reduction Builds Solvent Water into Oxygenate Products. Journal of the American Chemical Society, 2018, 140, 9337-9340.	6.6	170
54	Theory of thin-film-mediated exfoliation of van der Waals bonded layered materials. Physical Review Materials, 2018, 2, .	0.9	18

#	Article	IF	CITATIONS
55	Pressure–Temperature Phase Diagram of Vanadium Dioxide. Nano Letters, 2017, 17, 2512-2516.	4.5	65
56	Hydrogen evolution activity of individual mono-, bi-, and few-layer MoS 2 towards photocatalysis. Applied Materials Today, 2017, 8, 132-140.	2.3	32
57	Highly Stable Near-Unity Photoluminescence Yield in Monolayer MoS ₂ by Fluoropolymer Encapsulation and Superacid Treatment. ACS Nano, 2017, 11, 5179-5185.	7.3	86
58	Wide bandgap BaSnO3 films with room temperature conductivity exceeding 104 S cmâ^'1. Nature Communications, 2017, 8, 15167.	5.8	175
59	Optimizing C–C Coupling on Oxide-Derived Copper Catalysts for Electrochemical CO ₂ Reduction. Journal of Physical Chemistry C, 2017, 121, 14191-14203.	1.5	254
60	Phosphate tuned copper electrodeposition and promoted formic acid selectivity for carbon dioxide reduction. Journal of Materials Chemistry A, 2017, 5, 11905-11916.	5.2	46
61	Membraneless laminar flow cell for electrocatalytic CO ₂ reduction with liquid product separation. Journal Physics D: Applied Physics, 2017, 50, 154006.	1.3	22
62	Transparent Electrodes for Efficient Optoelectronics. Advanced Electronic Materials, 2017, 3, 1600529.	2.6	310
63	Pressurizing Field-Effect Transistors of Few-Layer MoS ₂ in a Diamond Anvil Cell. Nano Letters, 2017, 17, 194-199.	4.5	31
64	Al ₂ O ₃ Surface Complexation for Photocatalytic Organic Transformations. Journal of the American Chemical Society, 2017, 139, 269-276.	6.6	64
65	High figure-of-merit <i>p</i> -type transparent conductor, Cu alloyed ZnS <i>via</i> radio frequency magnetron sputtering. Journal Physics D: Applied Physics, 2017, 50, 505107.	1.3	19
66	A spongy nickel-organic CO ₂ reduction photocatalyst for nearly 100% selective CO production. Science Advances, 2017, 3, e1700921.	4.7	175
67	Efficient solar-driven electrochemical CO ₂ reduction to hydrocarbons and oxygenates. Energy and Environmental Science, 2017, 10, 2222-2230.	15.6	145
68	Strain-engineered growth of two-dimensional materials. Nature Communications, 2017, 8, 608.	5.8	253
69	Nucleation of melting and solidification in confined high aspect ratio thin films. Journal of Applied Physics, 2017, 122, 105304.	1.1	3
70	Measuring the Edge Recombination Velocity of Monolayer Semiconductors. Nano Letters, 2017, 17, 5356-5360.	4.5	19
71	Quantifying van der Waals Interactions in Layered Transition Metal Dichalcogenides from Pressure-Enhanced Valence Band Splitting. Nano Letters, 2017, 17, 4982-4988.	4.5	53
72	(Invited) Solar-Driven Electrochemical Conversion of Carbon Dioxide to Hydrocarbons and Oxygenates. ECS Meeting Abstracts, 2017, , .	0.0	0

#	Article	IF	CITATIONS
73	Surface origin and control of resonance Raman scattering and surface band gap in indium nitride. Journal Physics D: Applied Physics, 2016, 49, 255102.	1.3	6
74	Tailoring Copper Nanocrystals towards C ₂ Products in Electrochemical CO ₂ Reduction. Angewandte Chemie, 2016, 128, 5883-5886.	1.6	90
75	Goldâ€Mediated Exfoliation of Ultralarge Optoelectronicallyâ€Perfect Monolayers. Advanced Materials, 2016, 28, 4053-4058.	11.1	307
76	Tailoring Copper Nanocrystals towards C ₂ Products in Electrochemical CO ₂ Reduction. Angewandte Chemie - International Edition, 2016, 55, 5789-5792.	7.2	667
77	Pâ€Type Transparent Cuâ€Alloyed ZnS Deposited at Room Temperature. Advanced Electronic Materials, 2016, 2, 1500396.	2.6	40
78	CO ₂ Electroreduction with Enhanced Ethylene and Ethanol Selectivity by Nanostructuring Polycrystalline Copper. ChemElectroChem, 2016, 3, 1012-1019.	1.7	142
79	Pressure-induced structural transition of CdxZn1â^'xO alloys. Applied Physics Letters, 2016, 108, .	1.5	10
80	On the origin of photocarrier losses in Iron Pyrite nanocubes: Charge carrier dynamics and electrical transport study. , 2016, , .		0
81	Effects of temperature and gas–liquid mass transfer on the operation of small electrochemical cells for the quantitative evaluation of CO ₂ reduction electrocatalysts. Physical Chemistry Chemical Physics, 2016, 18, 26777-26785.	1.3	138
82	Undoped and Ni-Doped CoO _{<i>x</i>} Surface Modification of Porous BiVO ₄ Photoelectrodes for Water Oxidation. Journal of Physical Chemistry C, 2016, 120, 23449-23457.	1.5	52
83	Hydrolysis of Electrolyte Cations Enhances the Electrochemical Reduction of CO ₂ over Ag and Cu. Journal of the American Chemical Society, 2016, 138, 13006-13012.	6.6	640
84	Compliant substrate epitaxy: Au on <mml:math xmlns:mml="http://www.w3.org/1998/Math/MathML"><mml:msub><mml:mi>MoS</mml:mi><mml:mn>2Physical Review B, 2016, 93, .</mml:mn></mml:msub></mml:math 	:m n.x <td>nl:m2sub></td>	nl:m2sub>
85	Increased Optoelectronic Quality and Uniformity of Hydrogenated p-InP Thin Films. Chemistry of Materials, 2016, 28, 4602-4607.	3.2	12
86	General Thermal Texturization Process of MoS ₂ for Efficient Electrocatalytic Hydrogen Evolution Reaction. Nano Letters, 2016, 16, 4047-4053.	4.5	106
87	Air-Stable n-Doping of WSe ₂ by Anion Vacancy Formation with Mild Plasma Treatment. ACS Nano, 2016, 10, 6853-6860.	7.3	202
88	Activation Effect of Electrochemical Cycling on Gold Nanoparticles towards the Hydrogen Evolution Reaction in Sulfuric Acid. Electrochimica Acta, 2016, 209, 440-447.	2.6	32
89	High Luminescence Efficiency in MoS ₂ Grown by Chemical Vapor Deposition. ACS Nano, 2016, 10, 6535-6541.	7.3	140
90	Recombination Kinetics and Effects of Superacid Treatment in Sulfur- and Selenium-Based Transition Metal Dichalcogenides. Nano Letters, 2016, 16, 2786-2791.	4.5	233

#	Article	IF	CITATIONS
91	Opportunities to improve the net energy performance of photoelectrochemical water-splitting technology. Energy and Environmental Science, 2016, 9, 803-819.	15.6	75
92	Chemical Bath Deposition of p-Type Transparent, Highly Conducting (CuS) _{<i>x</i>} :(ZnS) _{1–<i>x</i>} Nanocomposite Thin Films and Fabrication of Si Heterojunction Solar Cells. Nano Letters, 2016, 16, 1925-1932.	4.5	89
93	Direct growth of single-crystalline Ill–V semiconductors on amorphous substrates. Nature Communications, 2016, 7, 10502.	5.8	45
94	High Photoluminescence Quantum Yield in Band Gap Tunable Bromide Containing Mixed Halide Perovskites. Nano Letters, 2016, 16, 800-806.	4.5	269
95	Trace Levels of Copper in Carbon Materials Show Significant Electrochemical CO ₂ Reduction Activity. ACS Catalysis, 2016, 6, 202-209.	5.5	143
96	Thinâ€Film Solar Cells with InP Absorber Layers Directly Grown on Nonepitaxial Metal Substrates. Advanced Energy Materials, 2015, 5, 1501337.	10.2	13
97	Low-temperature synthesized, p-type transparent conducting material for PV devices. , 2015, , .		1
98	Role of TiO ₂ Surface Passivation on Improving the Performance of p-InP Photocathodes. Journal of Physical Chemistry C, 2015, 119, 2308-2313.	1.5	127
99	Indirect Bandgap and Optical Properties of Monoclinic Bismuth Vanadate. Journal of Physical Chemistry C, 2015, 119, 2969-2974.	1.5	233
100	Moâ€Doped BiVO ₄ Photoanodes Synthesized by Reactive Sputtering. ChemSusChem, 2015, 8, 1066-1071.	3.6	100
101	p-Type Transparent Conducting Oxide/n-Type Semiconductor Heterojunctions for Efficient and Stable Solar Water Oxidation. Journal of the American Chemical Society, 2015, 137, 9595-9603.	6.6	122
102	Nonepitaxial Thin-Film InP for Scalable and Efficient Photocathodes. Journal of Physical Chemistry Letters, 2015, 6, 2177-2182.	2.1	33
103	Experimental demonstrations of spontaneous, solar-driven photoelectrochemical water splitting. Energy and Environmental Science, 2015, 8, 2811-2824.	15.6	520
104	Thin-Film Materials for the Protection of Semiconducting Photoelectrodes in Solar-Fuel Generators. Journal of Physical Chemistry C, 2015, 119, 24201-24228.	1.5	245
105	Near-unity photoluminescence quantum yield in MoS ₂ . Science, 2015, 350, 1065-1068.	6.0	993
106	Photocatalytic Stability of Single- and Few-Layer MoS ₂ . ACS Nano, 2015, 9, 11302-11309.	7.3	197
107	Thermal conductivity of isotopically controlled silicon nanostructures. New Journal of Physics, 2014, 16, 015021.	1.2	21
108	Atomic and electronic structures of lattice mismatched Cu2O/TiO2 interfaces. Applied Physics Letters, 2014, 104, 211605.	1.5	6

#	Article	IF	CITATIONS
109	Efficient and Sustained Photoelectrochemical Water Oxidation by Cobalt Oxide/Silicon Photoanodes with Nanotextured Interfaces. Journal of the American Chemical Society, 2014, 136, 6191-6194.	6.6	204
110	Photoactuators and motors based on carbon nanotubes with selective chirality distributions. Nature Communications, 2014, 5, 2983.	5.8	269
111	Robust production of purified H ₂ in a stable, self-regulating, and continuously operating solar fuel generator. Energy and Environmental Science, 2014, 7, 297-301.	15.6	85
112	BiVO ₄ thin film photoanodes grown by chemical vapor deposition. Physical Chemistry Chemical Physics, 2014, 16, 1651-1657.	1.3	77
113	Strain-Induced Indirect to Direct Bandgap Transition in Multilayer WSe ₂ . Nano Letters, 2014, 14, 4592-4597.	4.5	572
114	Life-cycle net energy assessment of large-scale hydrogen production via photoelectrochemical water splitting. Energy and Environmental Science, 2014, 7, 3264-3278.	15.6	195
115	Electronic Structure of Monoclinic BiVO ₄ . Chemistry of Materials, 2014, 26, 5365-5373.	3.2	356
116	Net primary energy balance of a solar-driven photoelectrochemical water-splitting device. Energy and Environmental Science, 2013, 6, 2380.	15.6	69
117	Reactive Sputtering of Bismuth Vanadate Photoanodes for Solar Water Splitting. Journal of Physical Chemistry C, 2013, 117, 21635-21642.	1.5	162
118	Amorphous Si Thin Film Based Photocathodes with High Photovoltage for Efficient Hydrogen Production. Nano Letters, 2013, 13, 5615-5618.	4.5	151
119	Quantum-coupled radial-breathing oscillations in double-walled carbon nanotubes. Nature Communications, 2013, 4, 1375.	5.8	54
120	Integrated microfluidic test-bed for energy conversion devices. Physical Chemistry Chemical Physics, 2013, 15, 7050.	1.3	20
121	Self-consistent mean-field theory of size distribution narrowing during ramped temperature ion beam synthesis. Journal of Applied Physics, 2013, 114, 234301.	1.1	1
122	Solar fuels production by artificial photosynthesis. , 2013, , .		0
123	A direct thin-film path towards low-cost large-area III-V photovoltaics. Scientific Reports, 2013, 3, 2275.	1.6	65
124	Vitamin D Deficiency Induces Early Signs of Aging in Human Bone, Increasing the Risk of Fracture. Science Translational Medicine, 2013, 5, 193ra88.	5.8	146
125	P-type InGaN across the entire alloy composition range. Applied Physics Letters, 2013, 102, 102111.	1.5	13
126	Interfacial free energies determined from binary embedded alloy nanocluster geometry. APL Materials, 2013, 1, 052105.	2.2	0

 $\mathsf{JOEL}\,\mathsf{W}\,\mathsf{AGER}$

#	Article	IF	CITATIONS
127	Few electron double quantum dot in an isotopically purified 28Si quantum well. Applied Physics Letters, 2012, 100, .	1.5	27
128	Nanoscale Probing of High Photovoltages at 109º Domain Walls. Ferroelectrics, 2012, 433, 123-126.	0.3	24
129	High optical quality polycrystalline indium phosphide grown on metal substrates by metalorganic chemical vapor deposition. Journal of Applied Physics, 2012, 111, 123112.	1.1	21
130	A direct comparison of non-destructive techniques for determining bridging stress distributions. Journal of the Mechanics and Physics of Solids, 2012, 60, 1462-1477.	2.3	11
131	pâ€Type InP Nanopillar Photocathodes for Efficient Solarâ€Driven Hydrogen Production. Angewandte Chemie - International Edition, 2012, 51, 10760-10764.	7.2	245
132	Copperâ€alloyed ZnS as a pâ€type transparent conducting material. Physica Status Solidi (A) Applications and Materials Science, 2012, 209, 2101-2107.	0.8	73
133	Taming transport in InN. Physica Status Solidi (A) Applications and Materials Science, 2012, 209, 83-86.	0.8	7
134	Semiconductor thin films directly from minerals—study of structural, optical, and transport characteristics of Cu2O thin films from malachite mineral and synthetic CuO. Thin Solid Films, 2012, 520, 3914-3917.	0.8	13
135	Efficient Photovoltaic Current Generation at Ferroelectric Domain Walls. Physical Review Letters, 2011, 107, 126805.	2.9	346
136	Size-Dependent Polar Ordering in Colloidal GeTe Nanocrystals. Nano Letters, 2011, 11, 1147-1152.	4.5	84
137	Effect of charged dislocation scattering on electrical and electrothermal transport in <mml:math xmlns:mml="http://www.w3.org/1998/Math/MathML" display="inline"><mml:mi>n</mml:mi>-type InN. Physical Review B, 2011, 84, .</mml:math 	1.1	59
138	Fatigue threshold R-curves predict small crack fatigue behavior of bridging toughened materials. Acta Materialia, 2011, 59, 7654-7661.	3.8	10
139	Limitations and Advantages of Raman Spectroscopy for the Determination of Oxidation Stresses. Oxidation of Metals, 2011, 75, 229-245.	1.0	29
140	Changes in cortical bone response to high-fat diet from adolescence to adulthood in mice. Osteoporosis International, 2011, 22, 2283-2293.	1.3	76
141	Photovoltaic action from In _x Ga _{1â€x} N pâ€n junctions with x > 0.2 grown on silicon. Physica Status Solidi C: Current Topics in Solid State Physics, 2011, 8, 2466-2468.	0.8	10
142	Rationally Designed, Threeâ€Dimensional Carbon Nanotube Backâ€Contacts for Efficient Solar Devices. Advanced Energy Materials, 2011, 1, 1040-1045.	10.2	27
143	Age-related changes in the plasticity and toughness of human cortical bone at multiple length scales. Proceedings of the National Academy of Sciences of the United States of America, 2011, 108, 14416-14421.	3.3	325
144	PN junction rectification in electrolyte gated Mg-doped InN. Applied Physics Letters, 2011, 99, .	1.5	19

#	Article	IF	CITATIONS
145	Mg doped InN and confirmation of free holes in InN. Applied Physics Letters, 2011, 98, 042104.	1.5	44
146	Modeling pulsed-laser melting of embedded semiconductor nanoparticles. Journal of Applied Physics, 2011, 110, 094307.	1.1	2
147	Reversible phase changes in Ge–Au nanoparticles. Applied Physics Letters, 2011, 98, 193101.	1.5	7
148	High quality InxGa1-xN thin films with x > 0.2 grown on silicon. Physica Status Solidi (B): Basic Research, 2010, 247, 1747-1749.	0.7	15
149	Above-bandgap voltages from ferroelectric photovoltaic devices. Nature Nanotechnology, 2010, 5, 143-147.	15.6	1,496
150	Nuclear Polarization of Phosphorus Donors in [sup 28]Si by Selective Optical Pumping. AIP Conference Proceedings, 2010, , .	0.3	2
151	Hole transport and photoluminescence in Mg-doped InN. Journal of Applied Physics, 2010, 107, .	1.1	67
152	Electron spin coherence of phosphorus donors in silicon: Effect of environmental nuclei. Physical Review B, 2010, 82, .	1.1	76
153	Progress on III-nitride/silicon hybrid multijunction solar cells. , 2010, , .		3
154	Embedded Binary Eutectic Alloy Nanostructures: A New Class of Phase Change Materials. Nano Letters, 2010, 10, 2794-2798.	4.5	27
155	Reduced size-independent mechanical properties of cortical bone in high-fat diet-induced obesity. Bone, 2010, 46, 217-225.	1.4	90
156	Osteopontin deficiency increases bone fragility but preserves bone mass. Bone, 2010, 46, 1564-1573.	1.4	169
157	On the effect of X-ray irradiation on the deformation and fracture behavior of human cortical bone. Bone, 2010, 46, 1475-1485.	1.4	171
158	Photoluminescence enhancement of Er-doped silica containing Ge nanoclusters. Applied Physics Letters, 2009, 95, .	1.5	6
159	Theory of Nanocluster Size Distributions from Ion Beam Synthesis. Physical Review Letters, 2009, 102, 146101.	2.9	17
160	Processing route for size distribution narrowing of ion beam synthesized nanoclusters. Applied Physics Letters, 2009, 95, 083120.	1.5	6
161	Homogeneous linewidth of the P31 bound exciton transition in silicon. Applied Physics Letters, 2009, 95, .	1.5	13
162	Structural Characterization of GeSn Alloy Nanocrystals Embedded in SiO ₂ . Materials Research Society Symposia Proceedings, 2009, 1184, 154.	0.1	1

Joel W Ager

#	Article	IF	CITATIONS
163	My Modeling Nanocluster Formation During Ion Beam Synthesis. Materials Research Society Symposia Proceedings, 2009, 1181, 60.	0.1	0
164	Highly luminescent InxGa1-xN thin films grown over the entire composition range by energetic neutral atom beam lithography & epitaxy (ENABLE). Physica Status Solidi C: Current Topics in Solid State Physics, 2009, 6, S409-S412.	0.8	5
165	Electrical properties of InGaNâ€&i heterojunctions. Physica Status Solidi C: Current Topics in Solid State Physics, 2009, 6, S413.	0.8	25
166	Stacking faults and phase changes in Mg-doped InGaN grown on Si. Physica Status Solidi C: Current Topics in Solid State Physics, 2009, 6, S421-S424.	0.8	4
167	Three-dimensional nanopillar-array photovoltaics on low-cost and flexible substrates. Nature Materials, 2009, 8, 648-653.	13.3	997
168	Electrical and electrothermal transport in InN: The roles of defects. Physica B: Condensed Matter, 2009, 404, 4862-4865.	1.3	11
169	Molecular beam epitaxy of InGaN thin films on Si(111): Effect of substrate nitridation. Thin Solid Films, 2009, 517, 6512-6515.	0.8	16
170	A Schottky topâ€gated twoâ€dimensional electron system in a nuclear spin free Si/SiGe heterostructure. Physica Status Solidi - Rapid Research Letters, 2009, 3, 61-63.	1.2	14
171	Photovoltaic effects in BiFeO3. Applied Physics Letters, 2009, 95, .	1.5	460
172	Demonstration of a Ill–Nitride/Silicon Tandem Solar Cell. Applied Physics Express, 2009, 2, 122202.	1.1	64
173	Aging and fracture of human cortical bone and tooth dentin. Jom, 2008, 60, 33-38.	0.9	85
174	Mgâ€doped InN and InGaN – Photoluminescence, capacitance–voltage and thermopower measurements. Physica Status Solidi (B): Basic Research, 2008, 245, 873-877.	0.7	55
175	Epitaxial growth of CdSexTe1â^'x thin films on Si(100) by molecular beam epitaxy using lattice mismatch graded structures. Journal of Crystal Growth, 2008, 310, 1081-1087.	0.7	18
176	The effect of aging on crack-growth resistance and toughening mechanisms in human dentin. Biomaterials, 2008, 29, 1318-1328.	5.7	121
177	Solid-state quantum memory using the 31P nuclear spin. Nature, 2008, 455, 1085-1088.	13.7	351
178	The true toughness of human cortical bone measured with realistically short cracks. Nature Materials, 2008, 7, 672-677.	13.3	453
179	Measurement of the toughness of bone: A tutorial with special reference to small animal studies. Bone, 2008, 43, 798-812.	1.4	180
180	Band gap bowing parameter of In1â^'xAlxN. Journal of Applied Physics, 2008, 104, .	1.1	67

#	Article	IF	CITATIONS
181	Evaluation of exhaled nitric oxide measurements in the emergency department for patients with acute asthma. Annals of Allergy, Asthma and Immunology, 2008, 100, 415-419.	0.5	4
182	Probing and modulating surface electron accumulation in InN by the electrolyte gated Hall effect. Applied Physics Letters, 2008, 93, .	1.5	31
183	InGaN Thin Films Grown by ENABLE and MBE Techniques on Silicon Substrates. Materials Research Society Symposia Proceedings, 2008, 1068, 1.	0.1	10
184	Structure map for embedded binary alloy nanocrystals. Applied Physics Letters, 2008, 93, 193114.	1.5	16
185	High electron mobility InN. Applied Physics Letters, 2007, 90, 162103.	1.5	29
186	Direct observation of the donor nuclear spin in a near-gap bound exciton transition: P31 in highly enriched S28i. Journal of Applied Physics, 2007, 101, 081724.	1.1	34
187	Kinetics of visible light photo-oxidation of Ge nanocrystals: Theory and in situ measurement. Applied Physics Letters, 2007, 90, 163118.	1.5	2
188	Defect Doping of InN. AIP Conference Proceedings, 2007, , .	0.3	0
189	Synthesis and Optical Properties of Multiband III-V Semiconductor Alloys. AIP Conference Proceedings, 2007, , .	0.3	0
190	The degree of bone mineralization is maintained with single intravenous bisphosphonates in aged estrogen-deficient rats and is a strong predictor of bone strength. Bone, 2007, 41, 804-812.	1.4	45
191	Shallow Impurity Absorption Spectroscopy in Isotopically Enriched Silicon. AIP Conference Proceedings, 2007, , .	0.3	2
192	Evidence for p-type InN. AIP Conference Proceedings, 2007, , .	0.3	2
193	Melting Kinetics of Confined Systems at the Nanoscale: Superheating and Supercooling. AIP Conference Proceedings, 2007, , .	0.3	0
194	The aminobisphosphonate risedronate preserves localized mineral and material properties of bone in the presence of glucocorticoids. Arthritis and Rheumatism, 2007, 56, 3726-3737.	6.7	34
195	p-type InN and In-rich InGaN. Physica Status Solidi (B): Basic Research, 2007, 244, 1820-1824.	0.7	23
196	Coherence of spin qubits in silicon. Journal of Physics Condensed Matter, 2006, 18, S783-S794.	0.7	107
197	Optical bleaching effect in InN epitaxial layers. Applied Physics Letters, 2006, 88, 191109.	1.5	22
198	Large Melting-Point Hysteresis of Ge Nanocrystals Embedded inSiO2. Physical Review Letters, 2006, 97, 155701.	2.9	108

#	Article	IF	CITATIONS
199	Structure and electronic properties of InN and In-rich group III-nitride alloys. Journal Physics D: Applied Physics, 2006, 39, R83-R99.	1.3	229
200	Optical Detection and Ionization of Donors in Specific Electronic and Nuclear Spin States. Physical Review Letters, 2006, 97, 227401.	2.9	63
201	Evidence forp-Type Doping of InN. Physical Review Letters, 2006, 96, 125505.	2.9	193
202	Multiband GaNAsP quaternary alloys. Applied Physics Letters, 2006, 88, 092110.	1.5	128
203	Analysis of Nano-scale Strain Near Shallow Trench Isolation Structures by Energy-filtered Convergent Beam Electron Diffraction. Microscopy and Microanalysis, 2006, 12, 938-939.	0.2	0
204	Isotopically engineered semiconductors: from the bulk to nanostructures. Physica Status Solidi (A) Applications and Materials Science, 2006, 203, 3550-3558.	0.8	18
205	Fracture and Ageing in Bone: Toughness and Structural Characterization. Strain, 2006, 42, 225-232.	1.4	39
206	Strategies for integration of donor electron spin qubits in silicon. Microelectronic Engineering, 2006, 83, 1814-1817.	1.1	13
207	Role of microstructure in the aging-related deterioration of the toughness of human cortical bone. Materials Science and Engineering C, 2006, 26, 1251-1260.	3.8	128
208	Dopants and defects in InN and InGaN alloys. Journal of Crystal Growth, 2006, 288, 278-282.	0.7	13
209	On the Increasing Fragility of Human Teeth With Age: A Deep-UV Resonance Raman Study. Journal of Bone and Mineral Research, 2006, 21, 1879-1887.	3.1	47
210	Structural properties of Ge nanocrystals embedded in sapphire. Journal of Applied Physics, 2006, 100, 114317.	1.1	22
211	Al2O3scale development on iron aluminides. Journal of Materials Research, 2006, 21, 1409-1419.	1.2	32
212	Analysis of Nanoscale Stress in Strained Silicon Materials and Microelectronics Devices by Energy-Filtered Convergent Beam Electron Diffraction. ECS Transactions, 2006, 2, 559-568.	0.3	2
213	Control of Defect Concentrations within a Semiconductor through Adsorption. Physical Review Letters, 2006, 97, 055503.	2.9	44
214	Photoluminescence of energetic particle-irradiated InxGa1â^'xN alloys. Applied Physics Letters, 2006, 88, 151101.	1.5	12
215	Fatigue threshold R-curves for predicting reliability of ceramics under cyclic loading. Acta Materialia, 2005, 53, 2595-2605.	3.8	52
216	Effects of polar solvents on the fracture resistance of dentin: role of water hydration. Acta Biomaterialia, 2005, 1, 31-43.	4.1	87

#	Article	IF	CITATIONS
217	Progress in Semiconductor Spectroscopy Using Isotopically Enriched Si. AIP Conference Proceedings, 2005, , .	0.3	3
218	Isotopic Effects in the Indirect Excitonic Transitions of Isotopically Enriched Silicon. AIP Conference Proceedings, 2005, , .	0.3	0
219	Relation Between Structural and Optical Properties of InN and InxGa1â^'xN Thin Films. AIP Conference Proceedings, 2005, , .	0.3	1
220	In Situ Characterization of Ge Nanocrystals Near the Growth Temperature. AIP Conference Proceedings, 2005, , .	0.3	0
221	Electron Transport Properties of InN. Materials Research Society Symposia Proceedings, 2005, 892, 91.	0.1	5
222	A Chemical Approach to 3-D Lithographic Patterning of Si and Ge Nanocrystals. Materials Research Society Symposia Proceedings, 2005, 901, 1.	0.1	0
223	Effect of native defects on optical properties of InxGa1â^'xN alloys. Applied Physics Letters, 2005, 87, 161905.	1.5	18
224	On the crystalline structure, stoichiometry and band gap of InN thin films. Applied Physics Letters, 2005, 86, 071910.	1.5	103
225	Compositional modulation in InxGa1â^'xN: TEM and X-ray studies. Microscopy (Oxford, England), 2005, 54, 243-250.	0.7	21
226	Mechanism of stress relaxation in Ge nanocrystals embedded in SiO2. Applied Physics Letters, 2005, 86, 063107.	1.5	52
227	High-Purity, Isotopically Enriched Bulk Silicon. Journal of the Electrochemical Society, 2005, 152, G448.	1.3	34
228	Pressure-dependent photoluminescence study of ZnO nanowires. Applied Physics Letters, 2005, 86, 153117.	1.5	83
229	Stable, freestanding Ge nanocrystals. Journal of Applied Physics, 2005, 97, 124316.	1.1	38
230	Nature of room-temperature photoluminescence in ZnO. Applied Physics Letters, 2005, 86, 191911.	1.5	274
231	Structure Sensitivity of Vibrational Spectra of Mesoporous Silica SBA-15 and Pt/SBA-15. Journal of Physical Chemistry B, 2005, 109, 17386-17390.	1.2	71
232	Effects of pressure on the band structure of highly mismatched Zn1â^'yMnyOxTe1â^'x alloys. Applied Physics Letters, 2004, 84, 924-926.	1.5	10
233	Group III-nitride alloys as photovoltaic materials. , 2004, , .		6
234	Effect of oxygen on the electronic band structure of II-O-VI alloys. , 2004, , .		1

#	Article	IF	CITATIONS
235	Oxygen induced band-gap reduction in ZnOxSe1â^'x alloys. Physica Status Solidi (B): Basic Research, 2004, 241, 603-606.	0.7	6
236	Pressure-dependent photoluminescence study of CuGaSe2. Physica Status Solidi (B): Basic Research, 2004, 241, 3117-3122.	0.7	4
237	Pressure dependence of optical transitions in semiconducting single-walled carbon nanotubes. Physica Status Solidi (B): Basic Research, 2004, 241, 3367-3373.	0.7	6
238	Optical properties and electronic structure of InN and In-rich group III-nitride alloys. Journal of Crystal Growth, 2004, 269, 119-127.	0.7	157
239	Band anticrossing in dilute nitrides. Journal of Physics Condensed Matter, 2004, 16, S3355-S3372.	0.7	34
240	Pressure dependence of the fundamental band-gap energy of CdSe. Applied Physics Letters, 2004, 84, 67-69.	1.5	70
241	Raman Spectroscopy and Time-Resolved Photoluminescence of BN and BxCyNzNanotubes. Nano Letters, 2004, 4, 647-650.	4.5	194
242	Synthetic Insertion of Gold Nanoparticles into Mesoporous Silica. Chemistry of Materials, 2003, 15, 1242-1248.	3.2	175
243	Universal bandgap bowing in group-III nitride alloys. Solid State Communications, 2003, 127, 411-414.	0.9	104
244	Narrow bandgap group III-nitride alloys. Physica Status Solidi (B): Basic Research, 2003, 240, 412-416.	0.7	25
245	Temperature dependence of the fundamental band gap of InN. Journal of Applied Physics, 2003, 94, 4457-4460.	1.1	375
246	Superior radiation resistance of In1â^'xGaxN alloys: Full-solar-spectrum photovoltaic material system. Journal of Applied Physics, 2003, 94, 6477-6482.	1.1	572
247	Band-gap bowing effects in BxGa1â ^{^*} xAs alloys. Journal of Applied Physics, 2003, 93, 2696-2699.	1.1	38
248	Effect of oxygen on the electronic band structure in ZnOxSe1â^'x alloys. Applied Physics Letters, 2003, 83, 299-301.	1.5	76
249	Encapsulation of Metal (Au, Ag, Pt) Nanoparticles into the Mesoporous SBA-15 Structure. Langmuir, 2003, 19, 4396-4401.	1.6	163
250	Structural and electronic properties of amorphous and polycrystalline In2Se3 films. Journal of Applied Physics, 2003, 94, 2390-2397.	1.1	48
251	Electrical and optical properties of GaN/Al2O3interfaces. Journal of Physics Condensed Matter, 2002, 14, 13337-13344.	0.7	18
252	An Ultravioletâ^'Raman Spectroscopic Investigation of Magnesium Chlorideâ^'Ethanol Solids with a 0.47 to 6 Molar Ratio of C2H5OH to MgCl2. Journal of Physical Chemistry B, 2002, 106, 2946-2949.	1.2	33

#	Article	IF	CITATIONS
253	Current status of research and development of IIIÂNÂV semiconductor alloys. Semiconductor Science and Technology, 2002, 17, 741-745.	1.0	61
254	Small band gap bowing in In1â [~] 'xGaxN alloys. Applied Physics Letters, 2002, 80, 4741-4743.	1.5	563
255	Unusual properties of the fundamental band gap of InN. Applied Physics Letters, 2002, 80, 3967-3969.	1.5	1,380
256	Band anticrossing in group II-Ox–VI1â^'x highly mismatched alloys: Cd1â^'xMnyOxTe1â^'x quaternaries synthesized by O ion implantation. Applied Physics Letters, 2002, 80, 1571-1573.	1.5	31
257	Band anticrossing effects in MgyZn1â^'yTe1â^'xSex alloys. Applied Physics Letters, 2002, 80, 34-36.	1.5	13
258	DX-like behavior of oxygen in GaN. Physica B: Condensed Matter, 2001, 302-303, 23-38.	1.3	13
259	Band Anticrossing in III-N-V Alloys. Physica Status Solidi (B): Basic Research, 2001, 223, 75-85.	0.7	119
260	Evolution of crystallinity of GaN layers grown at low temperature on sapphire with dimethylhydrazine and triethylgallium. Journal of Crystal Growth, 2001, 231, 89-94.	0.7	4
261	Formation of diluted III–V nitride thin films by N ion implantation. Journal of Applied Physics, 2001, 90, 2227-2234.	1.1	42
262	Synthesis of InNxP1â^'x thin films by N ion implantation. Applied Physics Letters, 2001, 78, 1077-1079.	1.5	46
263	Annealing of nonhydrogenated amorphous carbon films prepared by filtered cathodic arc deposition. Journal of Applied Physics, 2000, 88, 2395-2399.	1.1	48
264	Nitrogen-induced enhancement of the free electron concentration in sulfur implanted GaNxAs1â^'x. Applied Physics Letters, 2000, 77, 2858-2860.	1.5	29
265	Effect of Si doping on strain, cracking, and microstructure in GaN thin films grown by metalorganic chemical vapor deposition. Journal of Applied Physics, 2000, 87, 7745-7752.	1.1	233
266	Increased electrical activation in the near-surface region of sulfur and nitrogen coimplanted GaAs. Applied Physics Letters, 2000, 77, 3607-3609.	1.5	12
267	Interaction of Localized Electronic States with the Conduction Band: Band Anticrossing in II-VI Semiconductor Ternaries. Physical Review Letters, 2000, 85, 1552-1555.	2.9	195
268	Nature of the fundamental band gap in GaNxP1â^'x alloys. Applied Physics Letters, 2000, 76, 3251-3253.	1.5	228
269	Electron emission from films of carbon nanotubes and ta-C coated nanotubes. Applied Physics Letters, 1999, 75, 2680-2682.	1.5	53
270	Dependence of the fundamental band gap of AlxGa1â^'xN on alloy composition and pressure. Journal of Applied Physics, 1999, 85, 8505-8507.	1.1	112

Joel W Ager

#	Article	IF	CITATIONS
271	Reduction of band-gap energy in GaNAs and AlGaNAs synthesized by N+ implantation. Applied Physics Letters, 1999, 75, 1410-1412.	1.5	102
272	Light emission during fracture of a Zr–Ti–Ni–Cu–Be bulk metallic glass. Applied Physics Letters, 1999, 74, 3809-3811.	1.5	94
273	Effect of nitrogen on the band structure of GaInNAs alloys. Journal of Applied Physics, 1999, 86, 2349-2351.	1.1	153
274	Near-band-edge photoluminescence emission in AlxGa1â^'xN under high pressure. Applied Physics Letters, 1998, 72, 2274-2276.	1.5	14
275	Comparison study of photoluminescence from InGaN/GaN multiple quantum wells and InGaN epitaxial layers under large hydrostatic pressure. Applied Physics Letters, 1998, 73, 1613-1615.	1.5	11
276	Performance of Ultra Hard Carbon Wear Coatings on Microgears Fabricated by Liga. Materials Research Society Symposia Proceedings, 1998, 546, 115.	0.1	2
277	Pressure Induced Deep Gap State of Oxygen in GaN. Physical Review Letters, 1997, 78, 3923-3926.	2.9	223
278	Thermal stability of amorphous hard carbon films produced by cathodic arc deposition. Applied Physics Letters, 1997, 71, 3367-3369.	1.5	104
279	Heat treatment of cathodic arc deposited amorphous hard carbon films. Thin Solid Films, 1997, 308-309, 186-190.	0.8	53
280	Multilayer hard carbon films with low wear rates. Surface and Coatings Technology, 1997, 91, 91-94.	2.2	26
281	Diamond growth on hard carbon films. Diamond and Related Materials, 1996, 5, 1080-1086.	1.8	5
282	Hardness, elastic modulus, and structure of very hard carbon films produced by cathodicâ€arc deposition with substrate pulse biasing. Applied Physics Letters, 1996, 68, 779-781.	1.5	255
283	Effect of Si doping on the dislocation structure of GaN grown on the Aâ€face of sapphire. Applied Physics Letters, 1996, 69, 990-992.	1.5	166
284	Hardness and fracture toughness of bulk single crystal gallium nitride. Applied Physics Letters, 1996, 69, 4044-4046.	1.5	182
285	Quantitative stress mapping in alumina composites by optical fluorescence imaging. Acta Materialia, 1996, 44, 625-641.	3.8	21
286	Si in GaN — On the Nature of the Background Donor. Physica Status Solidi (B): Basic Research, 1996, 198, 243-249.	0.7	13
287	Effect of pretreatment process parameters on diamond nucleation on unscratched silicon substrates coated with amorphous carbon films. Journal of Applied Physics, 1996, 79, 485-492.	1.1	17
288	Site dependence of large oxygen isotope effect inY0.7Pr0.3Ba2Cu3O6.97. Physical Review B, 1996, 54, 14982-14985.	1.1	22

#	Article	IF	CITATIONS
289	Mechanical Properties of Amorphous Hard Carbon Films Prepared by Cathodic ARC Deposition. Materials Research Society Symposia Proceedings, 1995, 383, 453.	0.1	20
290	Fano interference of the Raman phonon in heavily boronâ€doped diamond films grown by chemical vapor deposition. Applied Physics Letters, 1995, 66, 616-618.	1.5	177
291	Residual Stress in Diamond and Amorphous Carbon Films. Materials Research Society Symposia Proceedings, 1995, 383, 143.	0.1	25
292	Effect of intrinsic growth stress on the Raman spectra of vacuumâ€arcâ€deposited amorphous carbon films. Applied Physics Letters, 1995, 66, 3444-3446.	1.5	102
293	Nickel, Morris, and Ager reply. Physical Review Letters, 1994, 72, 1389-1389.	2.9	0
294	High dose Cl implantation in ZnSe: Impurity incorporation and radiation damage. Journal of Applied Physics, 1994, 75, 1378-1383.	1.1	11
295	The nitrogen-hydrogen complex in ZnSe. Journal of Crystal Growth, 1994, 138, 1071-1072.	0.7	2
296	Spatially resolved measurement of lattice damage in alphaâ€particleâ€irradiated type IIa natural diamond by confocal photoluminescence microscopy. Journal of Applied Physics, 1994, 76, 4050-4053.	1.1	7
297	Local vibrational modes in Mg-doped gallium nitride. Physical Review B, 1994, 49, 14758-14761.	1.1	65
298	Direct evidence of carbon precipitates in GaAs and InP. Applied Physics Letters, 1994, 65, 1145-1147.	1.5	33
299	Local vibrational mode spectroscopy of nitrogenâ€hydrogen complex in ZnSe. Applied Physics Letters, 1993, 63, 2756-2758.	1.5	86
300	Temperature dependent mobility in singleâ€crystal and chemical vaporâ€deposited diamond. Journal of Applied Physics, 1993, 73, 2888-2894.	1.1	60
301	Optical characterization of sputtered carbon films (magnetic media overlayers). IEEE Transactions on Magnetics, 1993, 29, 259-263.	1.2	41
302	Quantitative measurement of residual biaxial stress by Raman spectroscopy in diamond grown on a Ti alloy by chemical vapor deposition. Physical Review B, 1993, 48, 2601-2607.	1.1	372
303	Particle―and photoinduced conductivity in typeâ€ŀla diamonds. Journal of Applied Physics, 1993, 74, 1086-1095.	1.1	68
304	Optimization of Ge/C ratio for compensation of misfit strain in solid phase epitaxial growth of SiGe layers. Applied Physics Letters, 1993, 63, 2682-2684.	1.5	36
305	Locus of pairing interaction inYBa2Cu3O7by site-selective oxygen isotope shift:O18inCuO2plane layers. Physical Review Letters, 1993, 70, 81-84.	2.9	54
306	Interface characterization of chemically vapor deposited diamond on titanium and Tiâ€6Alâ€4V. Journal of Applied Physics, 1993, 74, 7542-7550.	1.1	61

#	Article	IF	CITATIONS
307	The effect of coimplantation on the electrical activity of implanted carbon in GaAs. Journal of Applied Physics, 1993, 74, 7118-7123.	1.1	7
308	Combined surface characterization and tribological (friction and wear) studies of CVD diamond films. Journal of Materials Research, 1993, 8, 2577-2586.	1.2	21
309	Reducing Dislocation Density by Sequential Implantation of Ge and C in Si. Materials Research Society Symposia Proceedings, 1993, 298, 139.	0.1	0
310	Electrical Properties of Natural lia Diamonds Using Photo- and Particle Excitation. Materials Research Society Symposia Proceedings, 1993, 302, 245.	0.1	4
311	Characterization of Cvd Diamond Films by Optical Spectroscopies. Materials Research Society Symposia Proceedings, 1993, 302, 275.	0.1	0
312	Hydrogen-induced platelets in silicon: Infrared absorption and Raman scattering. Physical Review B, 1992, 45, 13363-13366.	1.1	64
313	Characterization of chemical bonding and physical characteristics of diamond-like amorphous carbon and diamond films. Journal of Materials Research, 1992, 7, 404-410.	1.2	70
314	Effects of substrate temperature on chemical structure of amorphous carbon films. Journal of Applied Physics, 1992, 71, 2243-2248.	1.1	133
315	Diamond growth on silicon nitride by microwave plasma chemical vapor deposition. Diamond and Related Materials, 1992, 1, 818-823.	1.8	8
316	Annealing studies of lowâ€ŧemperatureâ€grown GaAs:Be. Journal of Applied Physics, 1992, 71, 1699-1707.	1.1	111
317	Diamond synthesis by microwave plasma chemical vapor deposition using graphite as the carbon source. Applied Physics Letters, 1991, 59, 2386-2388.	1.5	33
318	Structure and mechanical properties of hydrogenated carbon films prepared by magnetron sputtering (for magnetic discs). IEEE Transactions on Magnetics, 1991, 27, 5160-5162.	1.2	53
319	Spatially resolved Raman studies of diamond films grown by chemical vapor deposition. Physical Review B, 1991, 43, 6491-6499.	1.1	288
320	Raman and resistivity investigations of carbon overcoats of thinâ€film media: Correlations with tribological properties. Journal of Applied Physics, 1991, 69, 5748-5750.	1.1	48
321	Laser heating effects in the characterization of carbon fibers by Raman spectroscopy. Journal of Applied Physics, 1990, 68, 3598-3608.	1.1	23
322	Raman intensities and interference effects for thin films adsorbed on metals. Journal of Chemical Physics, 1990, 92, 2067-2076.	1.2	18
323	Mapping materials properties with Raman spectroscopy utilizing a 2-D detector. Applied Optics, 1990, 29, 4969.	2.1	50
324	Gas phase kinetics of the reactions of NaO with H2, D2, H2O, and D2O. Journal of Chemical Physics, 1987, 87, 921-925.	1.2	27

#	Article	IF	CITATIONS
325	The kinetics of NaO + O ₂ + M and NaO + CO ₂ + M and their role in atmospheric sodium chemistry. Geophysical Research Letters, 1986, 13, 1395-1398.	1.5	17
326	Gas phase studies of Na diffusion in He and Ar and kinetics of Na+Cl2and Na+SF6. Journal of Chemical Physics, 1986, 84, 6161-6169.	1.2	24
327	Gas phase kinetics of the reactions of Na and NaO with O3 and N2O. Journal of Chemical Physics, 1986, 85, 5584-5592.	1.2	33
328	Laboratory studies of gas phase sodium diffusion. Journal of Chemical Physics, 1986, 85, 3469-3475.	1.2	7
329	High-Resolution Raman and Luminescence Spectroscopy of Isotope-Pure ²⁸ Si ¹² C, Natural and ¹³ C – Enriched 4H-SiC. Materials Science Forum, 0, 778-780, 471-474.	0.3	12